



The impact of TiO₂ on physical, optical characteristics and shielding qualities against γ -ray features of titanium bismo-borate glasses

Norah A. M. Alsaif¹ · Nada Alfryyan¹ · Hanan Al-Ghamdi¹ · Adel M. El-Refae² · R. A. Elsad³ · M. S. Shams^{2,4} · Y. S. Rammah⁵ · M. S. Sadeq^{6,7} · Shaaban M. Shaaban⁸ · Islam M. Nabil⁹

Received: 6 January 2024 / Accepted: 16 February 2024 / Published online: 29 March 2024

© The Author(s), under exclusive licence to Springer Science+Business Media, LLC, part of Springer Nature 2024

Abstract

In this study, the role of TiO₂ on the physical, and optical properties as well as the γ -ray protection features of a set of six glass samples with the chemical formula (65-X)B₂O₃–15BaO–5Bi₂O₃–15ZnO–XTiO₂, where X=0–10 mol% in the step of 2% have been investigated. The density (ρ) increased gradually from 3.70 to 3.93 g/cm³ and the molar volume (V_m) reduced from 27.71 to 26.72 cm³/mol as the TiO₂ content increased from 0 to 10 mol%. By the inclusion of TiO₂ in the glass networks, some absorption bands in the ultraviolet and visible regions are formed. Values of the indirect optical band gaps (E_g) were 2.550, 2.510, 2.470, 2.370, 2.270, and 2.180 eV for Ti-0.0, Ti-2.0, Ti-4.0, Ti-6.0, Ti-8.0, and Ti-10.0 glasses, respectively. The linear refractive index (n_0) calculated values varied from 2.515 to 2.631. The linear-attenuation coefficient (μ) followed the order: Ti-0.0 < Ti-2.0 < Ti-4.0 < Ti-6.0 < Ti-8.0 < Ti-10.0. The sample coded as Ti-10.0 glass sample (highest content of TiO₂) has the lowest half (HVL) and tenth (TVL) value layer. Within the investigated energy range of within the range: 51.590–19.480, 50.676–19.722, 50.696–19.833, 50.271–20.012, 49.860–20.193, and 49.460–20.376 for the prepared samples Ti-0.0, Ti-2.0, Ti-4.0, Ti-6.0, Ti-8.0, and Ti-10.0 glasses, respectively. Results confirmed that the suggested titanium bismo-borate glasses can be used in the optical field and as alternative materials for radiation shielding applications.

Keywords Titanium bismo-borate · Optical band gap · Radiation shielding · MCNP simulation code · RPE · PhX

1 Introduction

Glass is a class of material that combines optical transparency, simplicity in molding, and low cost, and they are used in a variety of applications as a result. The characteristics of glass can be improved by doping them with activator ions (Khattari et al. 2022a, 2022b; Rammah et al. 2022, 2020a; Alsaif et al. 2023a). Glass has demonstrated outstanding rare earth ion host properties as well as high mechanical and

thermal stability. Because of its use in cathode ray tubes, hybrid integrated circuits, magnetic heads, batteries, and solid oxide fuel cells, glass has a role in the solid-state ionic sector (Alrowaili et al. 2023; Alsaif et al. 2022, 2023b; Zakaly 2021).

Heavy metal oxide-containing ternary and quaternary glasses have been the subject of much investigation because of their use as ray absorbers, reflecting windows, mechanical sensors, and optical filters. Heavy metal oxide glasses also have strong chemical resistance and nonlinear optical characteristics (Hassaan et al. 2019; Arya and Singh 2015).

Borate glasses are a remarkable and intriguing glass system that, depending on changes in chemical composition, provides a variety of physical and chemical characteristics and has a wide range of uses. As a result, it can create different structural units in the glass network than silicon and phosphorus, which can only form tetrahedrally coordinated units with oxygens. Boron can modify its coordination with oxygens between three and four. Other than silicate glasses, borate glasses have received the most research attention. Gamma-ray protection, high-capacity reversible electrodes, preventing bacterial development, optical glasses, continuous filament fiberglass, and most recently as a bioactive material are just a few of the many uses for glasses containing B_2O_3 (Abdelghany and ElBatal 2013).

As glass modifiers, several heavy metal oxides (HMO) are introduced into the system of borate glasses to increase their chemical resistance and encourage the synthesis of more non-bridging oxygen (NBO) links; on the other hand, prior additions increase the sample density. These (HMO) include PbO , Bi_2O_3 , and MoO_3 (Sayyed et al. 2019). The mechanical and optical characteristics of the glasses are improved by adding barium carbonate ($BaCO_3$) (Mariselvam and R. Arun kumar. 2021; Mariselvam 2021; Misbah et al. 2022).

Due to its higher atomic number ($Z=56$), barium can enhance the gamma-ray attenuation property (Mariselvam 2022). Barium borate glasses have grown in significance as a result of their remarkable optical properties, high thermal conductivity, low melting point, excellent mechanical stability, and high transition metals (TMs) solubility (Marzouk et al. 2022; Aboud et al. 2022; Alsaif et al. 2023c).

The titanium-oxide-doped glasses have grown in significance recently among the numerous transition metal-oxide-doped glasses because of their potential use in non-linear optical devices such as ultrafast switches and power limiters. In silicate glasses, titanium oxide is typically thought of as a nucleating agent of crystallization. However, it has been shown that all other glass matrices include minor amounts of TiO_2 that improve the glass-forming capacity and chemical resistance of the glasses. Titanium ions frequently occur in glass networks in the Ti^{4+} state and take part in the formation of glass networks with the structural elements TiO_4 , TiO_6 , and occasionally TiO_5 (comprising trigonal bipyramids). Ti^{4+} ions' empty or unfilled d-shells are a bigger factor in the non-linear polarizabilities. Additionally, the study of the coordinated chemistry of titanium ions in alkali fluoroborate glass networks is intriguing in and of itself since the presence of these ions may significantly alter a variety of physical characteristics, such as color, chemical resistance, mechanical strength, and insulating qualities (Nageswara Rao et al. 2005). The Ti–O bond length ($\sim 1.96 \text{ \AA}$), which can significantly increase the non-linear polarizabilities of TiO_2 , is another intriguing characteristic of this material (Alajerami et al. 2013). As a glass forming, TiO_2 encourages something more polymerized structure and improves the stability of the glass concerning devitrification.

Six samples of titanium bismo-borate glasses with the chemical formula B_2O_3 – BaO – Bi_2O_3 – ZnO – TiO_2 were created for the current study. TiO_2 's impact on the

produced glass's structural, physical, optical, and gamma-ray efficacy has been studied for applications in radiation and optical protection.

2 Experimental work

2.1 Preparation of glasses

Using the conventional melt quenching method, the following glass samples were created: (65-X)B₂O₃-15BaO-5Bi₂O₃-15ZnO-XTiO₂, where X=0, 2, 4, 6, 8, and 10 mol% as shown in Table 1. The purity of all oxides, B₂O₃, BaCO₃, Bi₂O₃, ZnO, and TiO₂, was 99%. Weights totaling 10 g were produced for each composite combination. Powders were first precisely weighed by the molar ratio and thoroughly combined in a agate mortar for 30 min to guarantee optimum homogeneity. The resultant mixture was then put into exposed 50 mL porcelain crucibles, which were then pre-heated for 45 min at 300 °C in a usual setup. A clear, highly viscous liquid was created after it was transferred to another electric oven and roasted for 30 min at 1100–1150 °C The melting viscous was poured into cylinder stainless steel forms to produce glass discs. The produced glasses were normally annealed in a muffle furnace after being quenched, in which they are heated to 300 °C for 12 h to prevent bubble formation and thermal stress. Generally, the produced glasses are named Ti-X, and for each sample:

Ti-0.0: 65B₂O₃-15BaO-5Bi₂O₃-5ZnO-0.0TiO₂, with density 3.70 g cm⁻³,

Ti-2.0: 63B₂O₃-15BaO-5Bi₂O₃-15ZnO-2.0TiO₂, with density 3.77 g cm⁻³,

Ti-4.0: 61B₂O₃-15BaO-5Bi₂O₃-15ZnO-4.0TiO₂, with density 3.81 g cm⁻³,

Ti-6.0: 59B₂O₃-15BaO-5Bi₂O₃-15ZnO-6.0TiO₂, with density 3.84 g cm⁻³,

Ti-8.0: 57B₂O₃-15BaO-5Bi₂O₃-15ZnO-8.0TiO₂, with density 3.88 g cm⁻³, and.

Ti-10.0: 55B₂O₃-15BaO-5Bi₂O₃-15ZnO-10.0TiO₂, with density 3.93 g cm⁻³.

A photo of the produced Ti-X glasses is depicted in Fig. 1. As seen, as TiO₂ content increases, there is grading in color from yellowish brown to brown.

2.2 Measurements

The amorphous state of the prepared Ti-X glasses confirmed by X-ray diffraction (XRD) measurements (Bruker D8 Advance diffractometer) using Cu K_α radiation ($k=1.54 \text{ \AA}$) at 40 kV and 100 mA.

The Ti-X glasses' density (ρ) was measured through the Archimedes principle. A floating liquid Toluene with a density of $\rho_{\text{Toluene}}=0.865 \text{ g cm}^{-3}$ was used for the measurements. The density of each sample can be evaluated as follows:



Fig. 1 Photo of the prepared Ti-X glasses

$$\rho = \left(\frac{W_{\text{air}}}{W_{\text{air}} - W_{\text{Toluene}}} \right) \times \rho_{\text{Toluene}} \quad (1)$$

where W_{air} and W_{Toluene} represent to the weight of sample in air and Toluene liquid, respectively.

For every glass sample, the molar volume (V_m) is computed as follows:

$$V_m = \frac{M_{W_{\text{glass}}}}{\rho_{\text{glass}}} \quad (2)$$

where glass's molecular weight is expressed as $M_{W_{\text{glass}}}$.

A double-beam-spectrophotometer (type: Cary-5000 UV Vis NIR) was used at an ambient temperature to examine the UV and/or VIS absorption spectrum of Ti-X glasses.

2.3 Methods

2.3.1 MCNP5 simulation code

The γ -ray simulations of the studied Ti-X glasses were achieved by employing the Monte-Carlo simulation code-5 (MCNP) with a single energy point source in the photon energy (E) from 0.015 to 15 MeV ENDF/B.VI8 nuclear database (Brown et al. 2002). It simulates the transit of X/γ -rays, and neutrons while considering the physics interaction processes ((PE) photoelectric effect, (CS) compton scattering process, and (PP) pair production processes) (M.C. Team 2003; Mosorov and Abdullah 2011). The input files of the MCNP code need detailed data (e.g., source dimensions, sample elemental composition, etc.) to get accurate output results (Akkurt and Malidarré 2021). The experimental arrangement has considered all parameters. A cell card in a text file described the γ -source, primary collimator, sample, secondary collimator, and detector (Zhou et al. 2014). The γ -source was found to be a single-energy beam located 16 cm from the detector. The command tally F4:P determines the average track length of the incident γ -rays emitted from the simulated gamma source. A dynamic view of the radiation attenuation simulation system for the

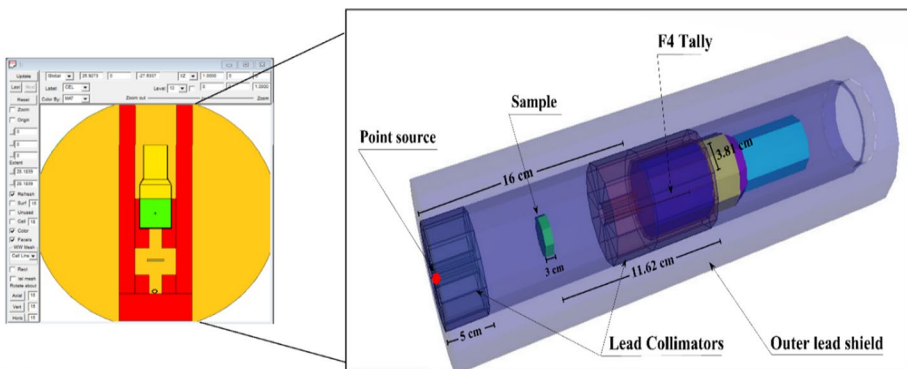


Fig. 2 The dynamic view of the radiation attenuation simulation system used for the prepared Ti-X glass samples

investigated Ti-X glasses is shown in Fig. 2. The samples were created as a cylinder geometry (diameter = 3 cm) and located between the source and the detection region (Zhou et al. 2014). The fabricated Ti-X glass samples' elemental composition was created in the input file's material card. A total of NPS = 10 million particles per run is used for all computations to achieve the minimum random statistical errors.

The intensity of the incident (I_0) and transmitted (I) γ -ray photons was measured for each Ti-X glass sample. The linear-attenuation (LAC = μ) coefficient can be calculated using Lambert-the following (Lakshminarayana et al. 2018; Kaky et al. 2023; Salem et al. 2023):

$$I = I_0 e^{-\mu x}, \quad (3)$$

where x is the thickness of the glass samples. An important sign of a material's characteristic is the mass-attenuation coefficient (MAC = μ_m), which is calculated as follows (Kaky et al. 2023):

$$\text{MAC} = \frac{\text{LAC}}{\rho}, \quad (4)$$

The μ parameter calculates the values needed to reduce the incident radiation to half or a tenth- of its original value. The half-value (HVL) and the tenth-value (TVL) layers can be calculated as follows (Salem et al. 2023; Mhareb et al. 2021):

$$\text{HVL} = \frac{\ln 2}{\mu} \quad (5)$$

$$\text{TVL} = \frac{2.303}{\text{LAC}} \quad (6)$$

The mean free path (MFP) is the average track distance photon movements before colliding with the attenuator using the following equation (Kaky et al. 2020):

$$\text{MFP} = \frac{1}{\mu} \quad (7)$$

Also, the radiation protection efficiency (RPE) is an important statistic to take into account when determining the level of attenuation that could be provided by various shielding materials. Also, the transfer factor (TF) is the factor that indicates the transmitted photons would be transferred through the Ti-X glasses, the RPE and TF factors can be calculated as follows (Kaky et al. 2019):

$$\text{RPE, \%} = \left(1 - \frac{I}{I_0}\right) 100 \quad (8)$$

$$\text{TF, \%} = \left(\frac{I}{I_0}\right) 100 \quad (9)$$

The effective atomic number (Z_{ef}): can be computed as (Alfryyan et al. 2023):

$$Z_{\text{ef}} = \frac{\sum_i f_i A_i (\mu_m)_i}{\sum_i \frac{A_i}{Z_i} (\mu_m)_i} \quad (10)$$

where f_i denotes the target element's fractional abundance. The average atomic mass of any material is $\sum f_i A_i$ structure. Z_i denotes the atomic number.

2.3.2 Phy-X (PhX) program

The Phy-X/PSD (PhX) is online free software used to calculate the MAC for the elements/compositions of any material (Sakar et al. 2020). In order to examine the samples under study, all of the radiation shielding parameters were chosen as output data (Sakar et al. 2020). The relative differences (φ , %) was also calculated by comparing the data obtained from PhX and MCNP as follows (Rammah et al. 2020b):

$$\varphi(\%) = \left| \frac{\text{MCNP} - \text{PhX}}{\text{MCNP}} \right| \times 100 \quad (11)$$

3 Results and discussion

3.1 XRD patterns

Figure 3 depicts the XRD patterns for the prepared Ti-X glasses. As shown in Fig. 3, the XRD patterns characterized by no sharp peaks and have a broadening peak in the range of $2\theta = 20^\circ - 30^\circ$. This observation demonstrated the amorphous nature of prepared glass samples.

Fig. 3 XRD patterns of the prepared Ti-X glasses

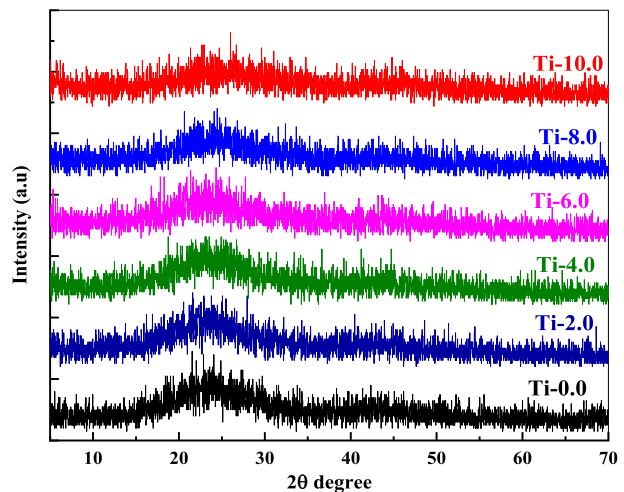
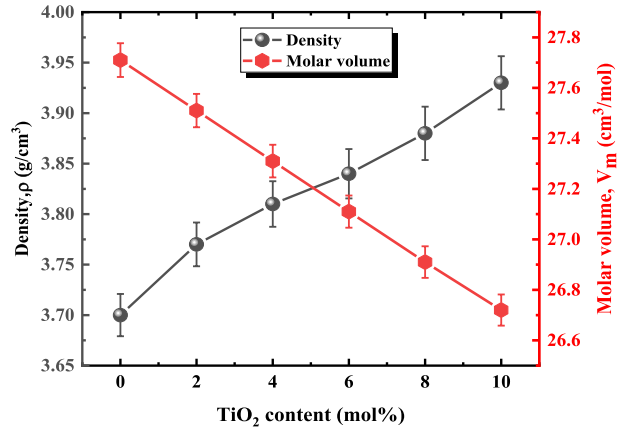


Fig. 4 Variation of density and molar volume as a function of TiO₂ content of the Ti-X glasses



3.2 Density and molar volume

In order to evaluate the geometric configurations of the glass network concerning variations in its structural compactness, the density (ρ) and molar volume (V_m) analysis are necessary. The ρ and V_m of the investigated Ti-X glass samples are influenced by the TiO₂ concentration. As seen in Fig. 4, the higher molar mass (79.899 g mol⁻¹) and density (4.230 g cm⁻³) of TiO₂ replaces the lower molar mass (69.620 g mol⁻¹) and density (2.460 g cm⁻³) of B₂O₃, causing the glass samples to increase in density as the TiO₂ content increases progressively (see Table 1). Furthermore, the significant improvement in density as TiO₂ content increases can be attributed to the conversion of certain BO₃ groups into BO₄ groups, which increases the amount of non-bridging oxygen bonds (NBOs) at the expense of bridging oxygen bonds (BO). In contrast, as the TiO₂ content increases, the V_m decreases. This suggests that as the ratio of TiO₂ increases, the structure becomes loosely packed.

3.3 Optical studies

Figure 5a represents the optical absorption spectra for Ti-0.0, Ti-2.0, Ti-4.0, Ti-6.0, Ti-8.0, and Ti-10.0 glasses within a wavelength range of 300–1100 nm. For more investigations, a comparison between the undoped glass samples with the glass sample comprising the highest concentrations of TiO₂ was presented in Fig. 5b. The optical absorption spectrum of the TiO₂-free glass sample (Ti-0.0) displays only one absorption band at about 380 nm (marked by * in Fig. 5b). Furthermore, this band is associated with the Bi cations as reported in Ref. (Mansour et al. 2021). After adding TiO₂ to the glass samples, some absorption bands in the ultraviolet and visible regions are formed. The inset of Fig. 5b displays the deconvolution of two absorption bands shown at 520 and 680 nm after the addition of TiO₂. These absorption bands can be explained as follows, titanium cations can exist in two oxidation states, specifically the trivalent (Ti³⁺) and the tetravalent (Ti⁴⁺) ions (Marzouk et al. 2016). Ti³⁺ cations have the 3d¹ electronic configurations and consequently display an absorption band at approximately 440–480 nm (labeled by # in Fig. 5b) and sometimes with distortion of Ti³⁺ cations, two absorption bands at about 540 and 680 nm are formed (Marzouk et al. 2016). The band at 540 nm can be ascribed to ²B_{2g} → ²B_{1g}, and the band 66 at 80 nm can

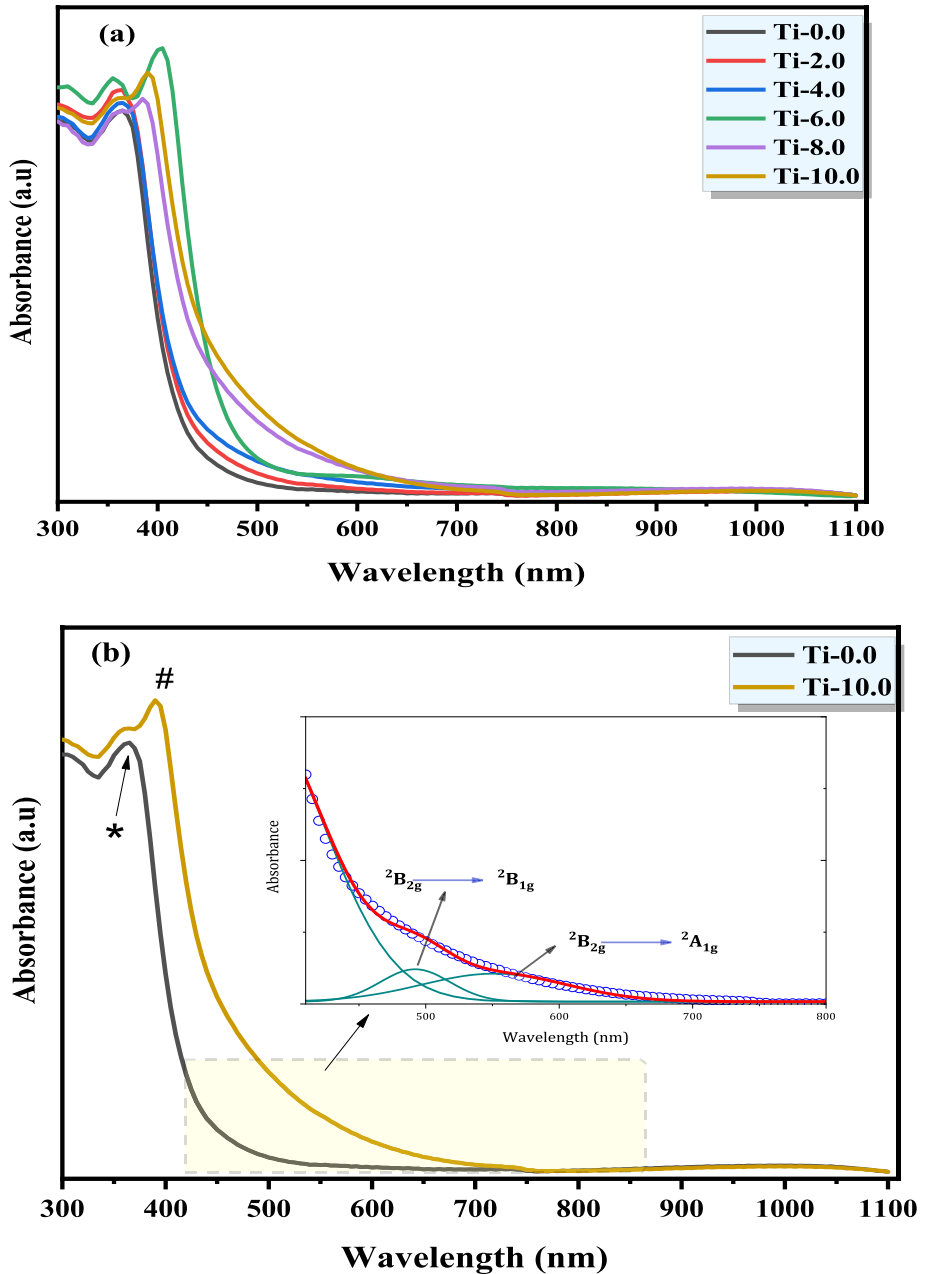


Fig. 5 **a** Optical absorbance as a function of wavelength for the prepared glass samples in UV–Vis–NIR regions from 300 to 1100 nm; **b** a comparison between the undoped glass sample with the glass sample comprising the highest concentrations of TiO₂, the inset represents the deconvoluted peaks for Ti³⁺ ions in tetragonal distorted octahedral sites

be associated with ${}^2B_{2g} \rightarrow {}^2A_{1g}$ electronic transitions of Ti³⁺ cations in tetragonal distorted octahedral symmetry (Alajerami et al. 1026). Moreover, tetravalent titanium (Ti⁴⁺) cations have *d0* electronic configurations and display no absorption bands in the visible range but only show ultraviolet absorption bands (Marzouk et al. 2016).

Furthermore, the optical band gaps (E_g) of these glass samples are determined by applying the Mott and Davis relationship (Davis and Mott 1970):

$$\alpha h\nu = \text{Constant}(h\nu - E_g)^n \tag{12}$$

where (α) is the absorption coefficient and ($h\nu$) is the photon energy. The exponent $n=2$ for the indirect allowed electronic transition, which relates to the majority of potential electronic transitions in amorphous materials, i.e., indirect band transitions, the most accurate computation of the transitions to the non-sharp absorption edge was found (Sadeq and Ibrahim 2021). h is the plank's constant and the absorption coefficient is α . In this study, we computed the optical band gaps (E_g) values for all glass specimens with varying TiO₂ concentrations by finding the intersection of the extrapolated linear section of the plots [$(\alpha h\nu)^{1/2}$ vs. ($h\nu$)] (also known as Tauc's plot (Tauc 1974)) with the x-axis [$(\alpha h\nu)^{1/2} = 0$], as shown in Fig. 6. The obtained values of E_g are 2.55, 2.51, 2.47, 2.37, 2.27, and 2.18 eV for Ti-0.0, Ti-2.0, Ti-4.0, Ti-6.0, Ti-8.0, and Ti-10.0 glasses, respectively. As depicted in Fig. 7, the shrinkage in E_g values with the added TiO₂ additives is ascribed to the increased contents of NBOs in the glassy matrix. Besides, the creation of NBO rather than BO results in an increase in disorder, which results in lesser values of band gap energies (Sayed et al. 2022).

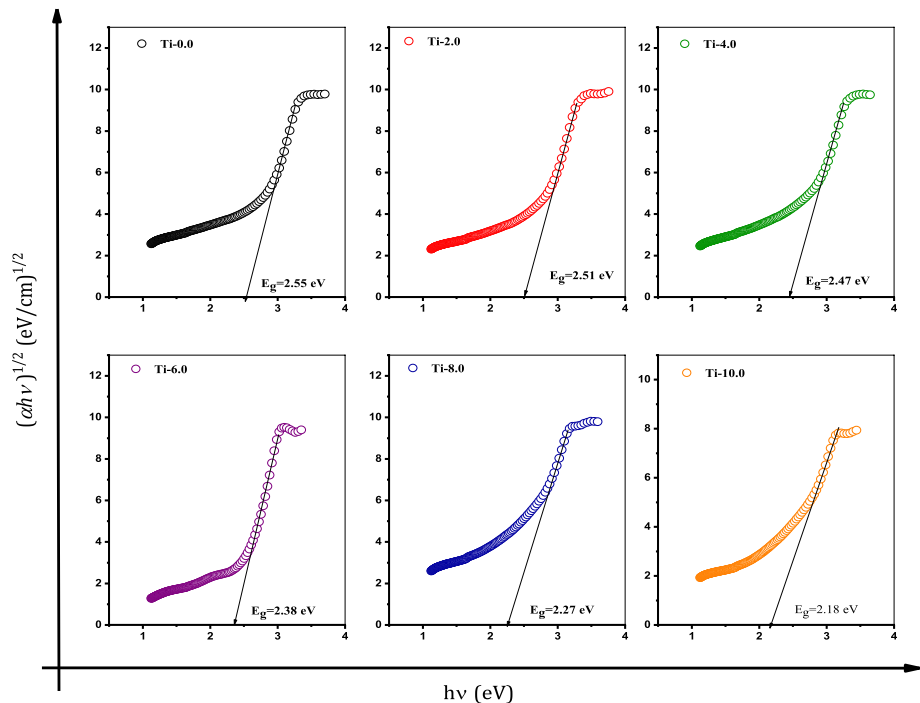


Fig. 6 Plot of $(\alpha h\nu)^{1/2}$ against $(h\nu)$ (Tauc's plot) for the prepared glass samples

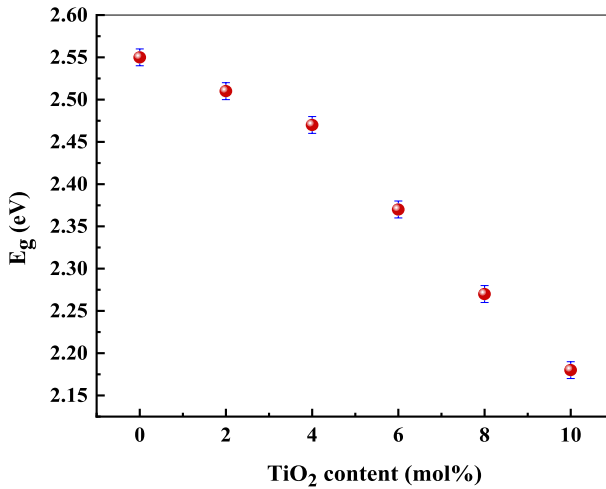


Fig. 7 The dependence of E_g values on TiO_2 content

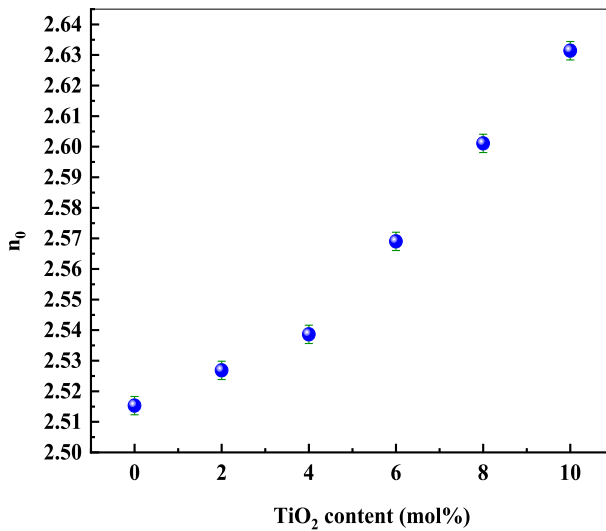


Fig. 8 The variations of refractive index (n_0) versus TiO_2 content

Additionally, the refractive index (n_0) of the Ti-X samples was calculated with the help of E_g values using Saad's formula (Negm et al. 2023),

$$n_0^2 = \sqrt{\frac{S^2}{E_g}} - 1 \quad (13)$$

where S^2 is a constant; $S^2 = 136.89$ eV. The calculated values of n_0 are 2.515, 2.527, 2.539, 2.569, 2.601 and 2.631 for Ti-0.0, Ti-2.0, Ti-4.0, Ti-6.0, Ti-8.0 and Ti-10.0 glasses,

Table 1 Samples code, glass composition, density, and molar volume of the prepared (65-X)B₂O₃-5Bi₂O₃-15ZnO-15BaO-XTiO₂; X=0, 2, 4, 6, 8, and 10 mol% glasses

Samples code	Glass composition	Density (g/cm ³)	Molar volume (cm ³ /mol)
Ti-0.0	65B ₂ O ₃ -5Bi ₂ O ₃ -15ZnO-15BaO	3.70	27.71
Ti-2.0	63B ₂ O ₃ -5Bi ₂ O ₃ -15ZnO-15BaO-2Ti ₂ O	3.77	27.51
Ti-4.0	61B ₂ O ₃ -5Bi ₂ O ₃ -15ZnO-15BaO-4Ti ₂ O	3.81	27.31
Ti-6.0	59B ₂ O ₃ -5Bi ₂ O ₃ -15ZnO-15BaO-6Ti ₂ O	3.84	27.11
Ti-8.0	57B ₂ O ₃ -5Bi ₂ O ₃ -15ZnO-15BaO-8Ti ₂ O	3.88	26.91
Ti-10.0	55B ₂ O ₃ -5Bi ₂ O ₃ -15ZnO-5BaO-10Ti ₂ O	3.93	26.72

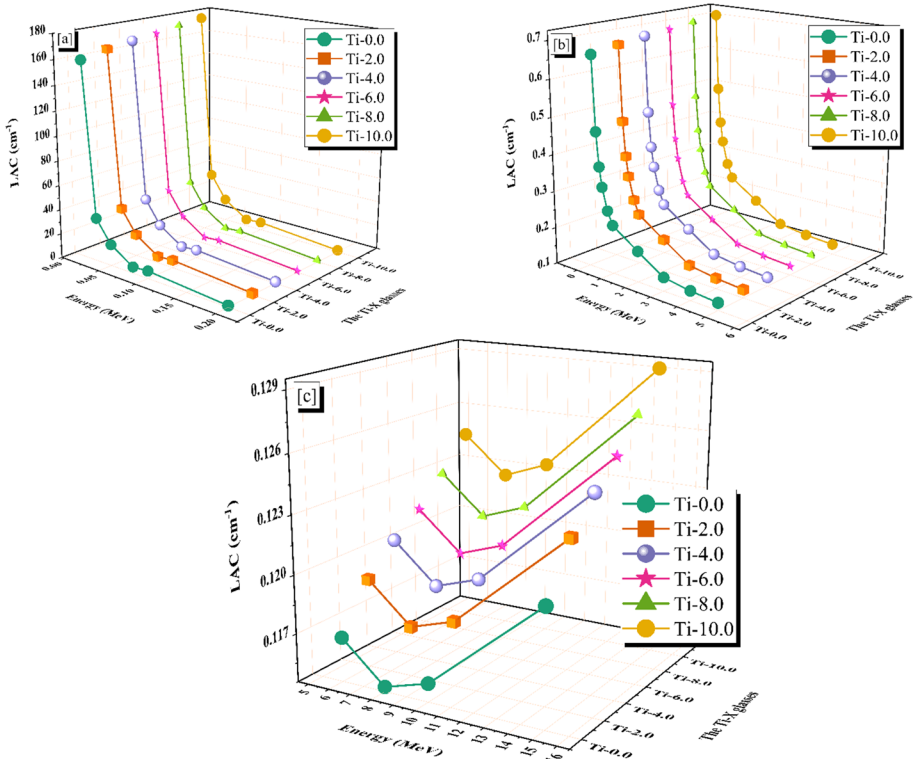


Fig. 9 Influence of gamma-ray energy on linear attenuation of **a** photoelectric, **b** compton scattering, and **c** pair production processes for the Ti-X glass samples

respectively and these values are offered in Fig. 8. These increases are ascribed to the diminished values of E_g values with higher NBO creation with the added TiO₂ from 0 to 10.0 mol%.

Table 2 The linear attenuation coefficient (*L_{Ac}*), which was obtained using MCNP and PhX for the prepared Ti-X: samples

Energy, (MeV)	The linear attenuation (<i>L_{Ac}</i> , cm ⁻¹)											
	Ti-0.0			Ti-2.0			Ti-4.0			Ti-6.0		
	PhX	MCNP	φ.(%)	PhX	MCNP	φ.(%)	PhX	MCNP	φ.(%)	PhX	MCNP	φ.(%)
0.015	164.178	159.670	2.823	168.362	164.174	2.551	170.847	166.874	2.381	173.089	169.231	2.280
0.03	35.602	35.282	0.907	36.314	36.019	0.819	36.849	36.569	0.765	37.233	36.963	0.732
0.05	17.759	17.308	2.604	18.025	17.611	2.353	18.290	17.897	2.196	18.435	18.055	2.103
0.08	5.387	5.171	4.172	5.466	5.267	3.770	5.545	5.356	3.519	5.587	5.405	3.369
0.1	6.344	6.138	3.360	6.425	6.236	3.036	6.518	6.339	2.834	6.562	6.389	2.713
0.2	1.350	1.312	2.906	1.369	1.334	2.626	1.387	1.354	2.451	1.397	1.365	2.347
0.3	0.685	0.670	2.175	0.696	0.682	1.965	0.704	0.692	1.834	0.709	0.697	1.756
0.4	0.480	0.472	1.610	0.488	0.481	1.455	0.493	0.487	1.358	0.497	0.491	1.300
0.5	0.386	0.380	1.411	0.392	0.387	1.275	0.397	0.392	1.190	0.400	0.395	1.139
0.6	0.332	0.328	1.242	0.337	0.334	1.032	0.341	0.338	0.963	0.344	0.341	0.922
0.8	0.270	0.267	0.969	0.275	0.27	0.876	0.278	0.276	0.817	0.280	0.278	0.782
1	0.234	0.232	0.888	0.238	0.24	0.803	0.241	0.276	0.749	0.243	0.241	0.717
2	0.185	0.183	0.879	0.188	0.19	0.794	0.190	0.189	0.741	0.192	0.191	0.709
3	0.137	0.137	0.554	0.140	0.14	0.500	0.142	0.141	0.467	0.143	0.142	0.447
4	0.126	0.126	0.419	0.129	0.13	0.379	0.130	0.130	0.353	0.131	0.131	0.338
5	0.120	0.120	0.339	0.123	0.12	0.306	0.124	0.124	0.286	0.125	0.125	0.274
6	0.117	0.117	0.430	0.120	0.12	0.388	0.121	0.121	0.362	0.122	0.122	0.347
8	0.115	0.115	0.366	0.117	0.12	0.331	0.119	0.119	0.309	0.120	0.120	0.296
10	0.116	0.115	0.177	0.118	0.12	0.160	0.119	0.119	0.149	0.121	0.120	0.143
15	0.121	0.120	0.068	0.123	0.12	0.062	0.125	0.125	0.058	0.126	0.126	0.055

Table 3 The linear attenuation coefficient (*LAc*), which was obtained using MCNP and PhX for the prepared Ti-X: X = 8.0 and 10.0 mol% samples

Energy, (MeV)	The linear attenuation coefficient (LAc cm ⁻¹)					
	Ti-8.0			Ti-10.0		
	PhX	MCNP	φ.(%)	PhX	MCNP	φ.(%)
0.015	175.794	172.177	2.101	178.969	175.506	1.973
0.03	37.716	37.463	0.675	38.298	38.057	0.634
0.05	18.628	18.274	1.937	18.870	18.533	1.820
0.08	5.644	5.475	3.104	5.716	5.554	2.916
0.1	6.623	6.462	2.500	6.701	6.547	2.348
0.2	1.410	1.380	2.162	1.427	1.399	2.031
0.3	0.716	0.705	1.618	0.725	0.714	1.520
0.4	0.502	0.496	1.198	0.508	0.502	1.125
0.5	0.404	0.400	1.050	0.409	0.405	0.986
0.6	0.347	0.344	0.850	0.352	0.349	0.798
0.8	0.283	0.281	0.721	0.286	0.284	0.677
1	0.245	0.243	0.661	0.248	0.246	0.621
2	0.194	0.193	0.654	0.196	0.195	0.614
3	0.144	0.144	0.412	0.146	0.145	0.387
4	0.133	0.132	0.312	0.134	0.128	0.293
5	0.127	0.126	0.252	0.128	0.125	0.237
6	0.123	0.123	0.320	0.125	0.123	0.300
8	0.121	0.121	0.273	0.123	0.123	0.256
10	0.122	0.122	0.132	0.124	0.124	0.124
15	0.127	0.127	0.051	0.129	0.129	0.048

3.4 Shielding qualities against gamma-ray

Figure 9a–c represents the LAC of the fabricated Ti-X glass samples. Tables 2 and 3 represent the μ values using MCNP code and PhX software in the γ -energy range of 0.015–15 MeV. The values of simulated μ are in decent agreement with the values calculated by PhX with a maximum ϕ of 4.118%. The μ values of the fabricated Ti-X glass samples decrease as the γ -energy increases. The simulated μ values drop from 159.670 to 0.120 cm⁻¹ for Ti-0.0, from 164.174 to 0.123 cm⁻¹ for Ti-2.0, from 166.874 to 0.125 cm⁻¹ for Ti-4.0, from 169.231 to 0.126 cm⁻¹ for Ti-6.0, from 172.177 to 0.127 cm⁻¹ for Ti-8.0 glass sample, and from 175.506 to 0.129 cm⁻¹ for Ti-10.0 glass sample at photon energy range from 0.015 to 15 MeV.

Figure 9a shows that there is a tough reduction in the μ values for all the fabricated Ti-X glass samples because of the PE interaction, which has changed in the cross-section with the interaction cross-section decreases strongly with the enrichment of E_γ values associated with a similar reduction in the PE interactions. The increase of the applied E_γ values between 0.015: 0.2 MeV causes a tough exponential decreasing tendency from 159.670 to 1.312 cm⁻¹ for Ti-0.0, from 164.174 to 1.334 cm⁻¹ for Ti-2.0, from 166.874 to 1.354 cm⁻¹ for Ti-4.0, from 169.231 to 1.365 cm⁻¹ for Ti-6.0, from 172.177 to 1.380 cm⁻¹ for Ti-8.0 glass sample, and from 175.506 to 1.399 cm⁻¹ for Ti-10.0 glass sample.

As shown in Fig. 9b, the simulated μ values in the energy photon interval from 0.3: 5 MeV undergo an exponential drop due to the enrichment of $E_\gamma > 0.2$ MeV. The CS

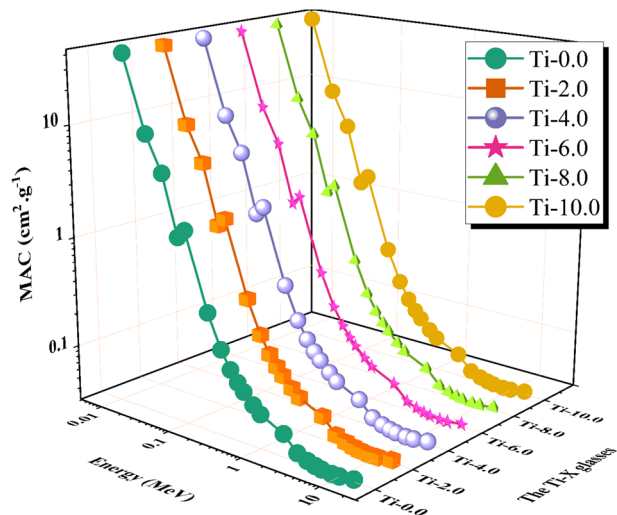
interaction with changes in cross-section caused by E_γ^{-1} is blamed for the exponential decline (Khattari et al. 2024; Shahboub et al. 2023). It is explained by higher energy photons' lower propensity to interact with the material's atoms results from their greater velocity. As a result, when energy increases, the likelihood of photon absorption falls, and the likelihood of photon scattering increases (Saleh et al. 2022). The enrichment in E_γ values was linked to a smooth decrease in the cross-section with drops in the quantity of photon-electron interactions, followed by a smooth drop in the μ values. The reduction in μ was from 0.670 to 0.120 cm^{-1} for Ti-0.0, from 0.682 to 0.122 cm^{-1} for Ti-2.0, from 0.692 to 0.124 cm^{-1} for Ti-4.0, from 0.697 to 0.125 cm^{-1} for Ti-6.0, from 0.705 to 0.126 cm^{-1} for Ti-8.0 glass sample, and from 0.714 to 0.128 cm^{-1} for Ti-10.0 glass sample with raising the E_γ values between 0.3: 5 MeV, respectively.

Also, there is a slight increase due to the PP interaction with cross-section changes with E_γ^2 (Ekinici et al. 2022) as seen in Fig. 9c. The μ were from 0.117 to 0.120 cm^{-1} for Ti-0.0, from 0.119 to 0.123 cm^{-1} for Ti-2.0, from 0.121 to 0.125 cm^{-1} for Ti-4.0, from 0.122 to 0.126 cm^{-1} for Ti-6.0, from 0.123 to 0.127 cm^{-1} for Ti-8.0 glass sample, and from 0.125 to 0.129 cm^{-1} for Ti-10.0 glass sample with raising the E_γ values between 6: 15 MeV. From the previous results, the addition of the TiO_2 to the zinc sodium lead borated glasses increases the values of the LAC values significantly. In comparison to the other samples, Ti-10.0 has the greatest μ values due to the concentration of TiO_2 (10 mol%) as well as the high density (3.930 g cm^{-3}).

The mass attenuation coefficient (MAC) of the Ti-X glasses behaves similarly to the μ . The MAC was varied from 43.154 to 0.033 $\text{cm}^2 \text{ g}^{-1}$ for Ti-0.0, from 43.547 to 0.033 $\text{cm}^2 \text{ g}^{-1}$ for Ti-2.0, from 43.799 to 0.033 $\text{cm}^2 \text{ g}^{-1}$ for Ti-4.0, from 44.070 to 0.033 $\text{cm}^2 \text{ g}^{-1}$ for Ti-6.0, from 44.376 to 0.033 $\text{cm}^2 \text{ g}^{-1}$ for Ti-8.0 sample, and from 44.658 to 0.033 $\text{cm}^2 \text{ g}^{-1}$ for Ti-10.0 glass sample as realized in Fig. 10.

Figure 11a and b show a comparison of the μ_m and μ between the fabricated glasses and those of commercial concrete (H-serpentine, I-limonite, B-magnetite, Ilmenite, S-scrap, and S-magnetite concretes (Bashter 1997) and some common glasses (RS-253-G18 (Zahran et al. 2022), and TZNNd9 (Zakaly et al. 2023)) at chosen energies 0.5, 5 and 10 MeV. At 0.5, 5, and 10 MeV, the μ of the Ti-10 glass sample have higher values than those of

Fig. 10 The mass attenuation coefficients (μ_m) v.s. the photon energy for the prepared Ti-X glass samples



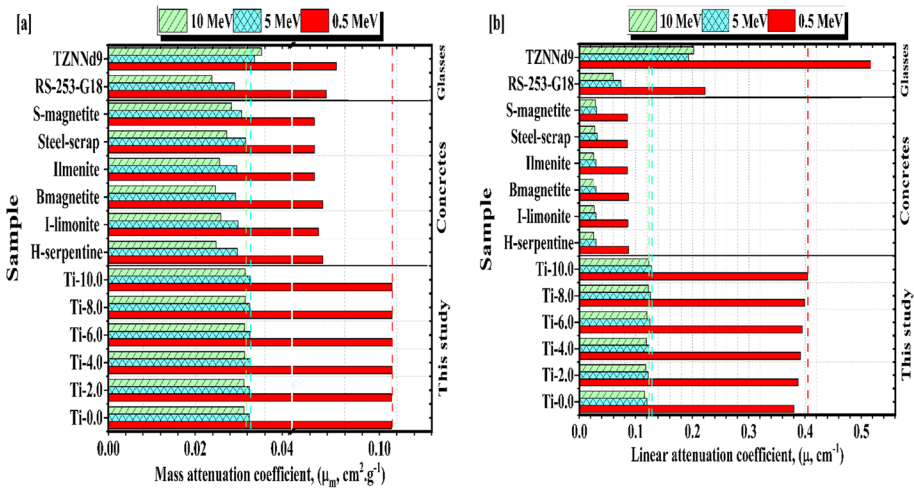


Fig. 11 **a** The mass attenuation coefficients, (μ_m , $\text{cm}^2 \text{g}^{-1}$), and **b** the linear attenuation coefficients (μ , cm^{-1}) for the Ti-X glass samples with reference concert and glass samples

concretes and glasses but the TZNNd9 glass sample. At 5, and 10 MeV, the μ_m of the Ti-10 glass sample have higher values than those of concretes and glasses but the TZNNd9 glass sample. At 0.5 MeV, the μ_m of the Ti-10 glass sample have higher values than those of concretes and glasses samples.

The half- and tenth-value layer (HVL, TVL) and mean free path (MFP) are ordinary measures of radiation protection efficiency. For a given E_γ , a stronger radiation shielding performance is often seen with a lower value for either parameter, as radiation is attenuated as it travels through a narrower zone (Saleh et al. 2022). Figure 12a–c presents the values of HVL, TVL, and MF computed by Eqs. (5), (6), and (7). The HVL of investigated Ti-X glass samples increased as the μ values decreased. The HVL values grew from 0.004 to 5.755 cm for Ti-0.0, from 0.004 to 5.636 cm for Ti-2.0, from 0.004 to 5.564 cm for Ti-4.0, from 0.004 to 5.509 cm for Ti-6.0, from 0.004 to 5.440 cm for Ti-8.0 sample, and from 0.004 to 5.359 cm for Ti-10.0 glass sample with raising the energy values from 0.015: 15 MeV, respectively as seen in Fig. 12a. The TVL values take the same trend as the HVL as seen in Fig. 12b. The variations of MFP with photon energy are illustrated in Fig. 12c. The MFP values range from 0.006 to 8.302 cm for Ti-0.0, from 0.006 to 8.131 cm for Ti-2.0, from 0.006 to 8.027 cm for Ti-4.0, from 0.006 to 7.947 cm for Ti-6.0, from 0.006 to 7.848 cm for Ti-8.0 sample, and from 0.006 to 7.732 cm for Ti-10.0 glass sample, respectively. Based on the results, it was discovered that the quantity of TiO₂ affected the HVL, TVL, and MFP values. This means that the Ti-10.0 glass sample had the lowest HVL, TVL, and MFL values, while the Ti-0.0 sample had the highest values. This suggests that the TiO₂ plays a role in the γ -rays attenuation performance of the Ti-X glasses.

Figures 13 and 14 show the transfer factor (TF) and the RPE of the Ti-X glasses. It shows that the RPE values are close to 100% at very low gamma ray energy (up to 0.015 MeV). When the gamma-photon energy was increased, the penetrating strength of the delivered photons also increased, leading to a significant decrease in the RPE levels. Therefore, increasing the gamma-photon energy decreases the photon-electron interactions within the manufactured glasses. The number of scattered photons increases once the photon-electron interaction is reduced, which has a detrimental effect on the RPE for the Ti-X

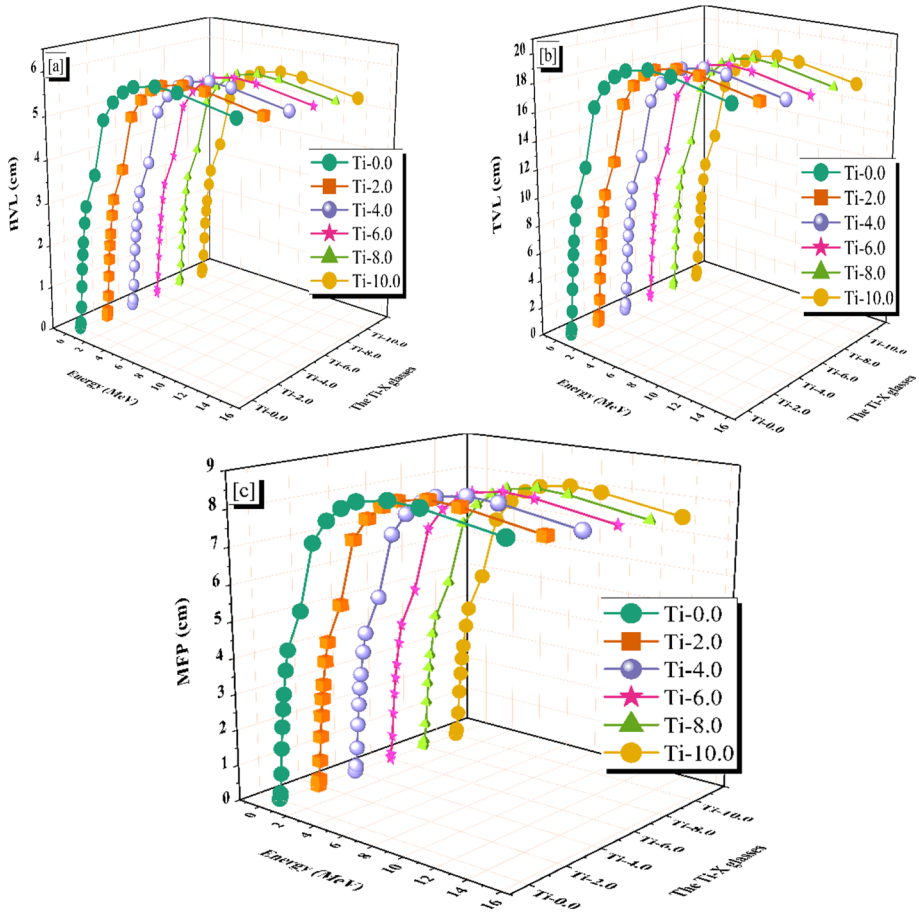


Fig. 12 **a** The half value layer (HVL), **b** the tenth value layer (TVL), and the mean free path (MF) for the prepared glass Ti-X samples vs. the photon energy

Fig. 13 The transfer factor (TF) for the prepared Ti-X glass samples vs. photon energy

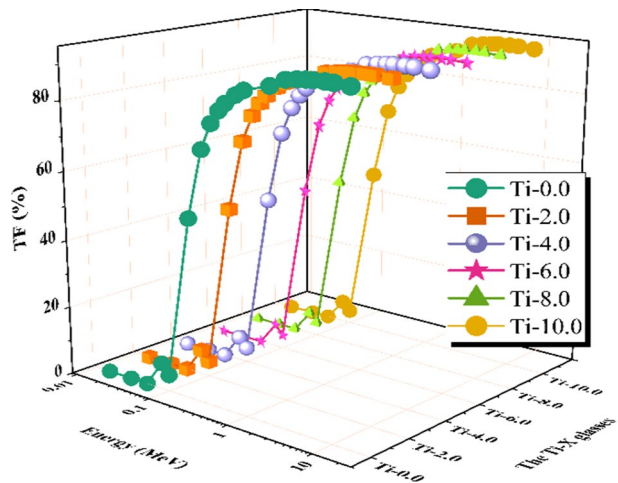


Fig. 14 The radiation protection efficiency (RPE) for the prepared Ti-X glass samples versus photon energy

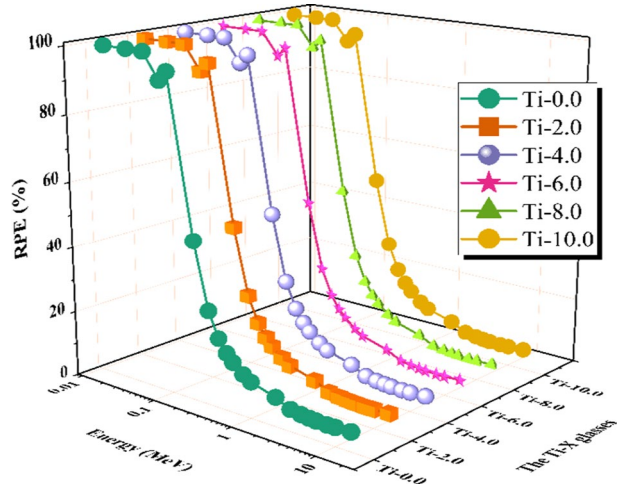
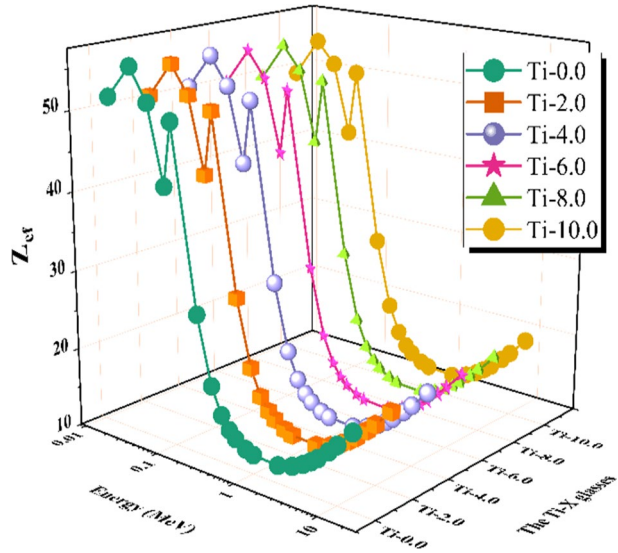


Fig. 15 The effective atomic number (Z_{ef}) obtained from PhX for the prepared Ti-X glass samples vs. photon energy



glass samples. For example, The RPE values dropped from ≈ 100.000 at 0.015 for all Ti-X glass samples to 5.845%, 5.964%, 6.039%, 6.098%, 6.172%, and 6.262% respectively, for Ti-X glass samples where X=0.0, 0.2, 0.4, 0.6, 0.8, and 10.0, respectively at gamma-ray energy 15 MeV. The results confirm a great shielding capacity for the Ti-X glass sample in the energy range from 0.015 to 0.1 MeV. Also, the Ti-X glass sample shows a good shielding capacity above 0.020–15 MeV.

The Z_{ef} , the effective atomic number of a composite, is a crucial metric that has many practical uses in contemporary technology, engineering, and physics. The value of Z_{ef} explains the different characteristics of a material. The relationship between the Z_{ef} and the E_γ for the glasses under study is shown in Fig. 15. Increases in Z_{ef} value are often indicative of enhanced radiation interaction, especially through the compton effect and photoelectric effect, in a given material. Consequently, high Z_{ef} -value materials may

better block high-energy radiation (Mostafa et al. 2021; Ibrahim et al. 2024; Nabil et al. 2023; Dh Hassib et al. 2019; Kaky and Sayyed 2024; Lakshminarayana et al. 2016; Kaky et al. 2017). It shows that different materials may be more or less successful in attenuating radiation depending on the energy of the radiation, with greater and lower MeV requiring different materials. For the energy spectrum of interest, the range of Z_{ef} of the fabricated Ti-X glass varied from 51.590 to 19.480, 50.676 to 19.722, 50.696 to 19.833, 50.271 to 20.012, 49.860 to 20.193, and 49.460 to 20.376 for the prepared samples Ti-0.0, Ti-2.0, Ti-4.0, Ti-6.0, Ti-8.0, and Ti-10.0 glasses, respectively. The Ti-0.0 has the lowest Z_{ef} values among the Ti-X six glasses. The Ti-10.0 glass sample has the highest Z_{ef} values among the energy range from 0.015: 15 MeV due to the high doping with the $TiO_2 = 10 \text{ mol}\%$.

4 Conclusion

Using the conventional melt quenching method, the glass samples with the chemical formula $(65-X)B_2O_3-15BaO-5Bi_2O_3-15ZnO-XTiO_2$, where $X=0, 2, 4, 6, 8,$ and $10 \text{ mol}\%$ have been prepared. Samples densities, molar volume, and optical characteristics of the prepared glasses have been investigated. Also, the gamma-ray protection features of the investigated glasses have been evaluated. The glass's densities were increased gradually from 3.70 to 3.93 g cm^{-3} and the molar volume was decreased from 27.71 to $26.72 \text{ cm}^3 \text{ mol}^{-1}$ as the TiO_2 content increased from 0 to $10 \text{ mol}\%$. After adding TiO_2 to the glass samples, some absorption bands in the ultraviolet and visible regions are formed. The obtained values of indirect optical band gaps (E_g) were $2.55, 2.51, 2.47, 2.37, 2.27,$ and 2.18 eV for Ti-0.0, Ti-2.0, Ti-4.0, Ti-6.0, Ti-8.0 and Ti-10.0 glasses, respectively. The calculated values of n_0 were $2.515, 2.527, 2.539, 2.569, 2.601,$ and 2.631 for Ti-0.0, Ti-2.0, Ti-4.0, Ti-6.0, Ti-8.0, and Ti-10.0 glasses, respectively. The linearattenuationcoefficient/s order is: $Ti-0.0 < Ti-2.0 < Ti-4.0 < Ti-6.0 < Ti-8.0 < Ti-10.0$. The prepared Ti-10.0 glass sample (highest content of TiO_2) has the lowest HVL, TVL, and MFP. The prepared Ti-10.0 glass sample presents the best gamma radiation shielding capability among the prepared Ti-X glasses. The obtained results confirmed that the suggested titanium bismorbate glasses can be used in the optical field and as alternative materials for radiation shielding applications.

Acknowledgements The authors express their gratitude to Princess Nourah bint Abdulrahman University Researchers Supporting Project number (PNURSP2024R60), Princess Nourah bint Abdulrahman University, Riyadh, Saudi Arabia. The authors extend their appreciation to the Deanship of Scientific Research at Northern Border University, Arar, KSA for funding this research work through the project number "NBU-FFR-2024-289-02".

Authors' contributions NAMA, NA, HAA, AME, RAE, MSS, YSR, MSS, IMN: conceptualization, methodology, software, validation, investigation, data curation, writing-review and editing, visualization, supervision.

Funding Princess Nourah bint Abdulrahman University Researchers Supporting Project number (PNURSP2024R60), Princess Nourah bint Abdulrahman University, Riyadh, Saudi Arabia.

Data availability All data generated or analyzed during this study are included in this published article.

Declarations

Conflict of interest The authors declare that they have no conflict of interest.

Ethical approval Authors declare that this manuscript is original, has not been published before, and is not currently being considered for publication elsewhere.

Consent to participate Not applicable.

Consent to publish Not applicable.

References

- Abdelghany, A.M., ElBatal, H.A.: Effect of TiO₂ doping and gamma ray irradiation on the properties of SrO–B₂O₃ glasses. *J. Non-Cryst. Solids* **379**, 214–219 (2013)
- Aboud, H., Aldhuaibata, M.J.R., Alajermi, Y.: Radiation shielding traits of bismuth–cadmium–barium–borate glasses: role of lead activation. *J. Phys. Chem. Solids* **164**, 110597–110608 (2022)
- Akkurt, I., Malidarre, R.B.: Gamma photon-neutron attenuation parameters of marble concrete by MCNPX code. *Radiat. Eff. Defects Solids* **176**, 906–918 (2021)
- Alajerami, Y.S.M., Hashim, S., Ghoshal, S.K., Saleh, M.A., Kadni, T., Saripan, M.I., Alzimami, K., Ibrahim, Z., Bradley, D.A.: The effect of TiO₂ and MgO on the thermoluminescence properties of a lithium potassium borate glass system. *J. Phys. Chem. Solids* **74**, 1816–1822 (2013)
- Alajerami, Y.S.M., Hashim, S., Hassan, W.M.S.W., Ramli, A.T.: The effect of titanium oxide on the optical properties of lithium potassium borate glass. *J. Mol. Struct.* **1026**, 159–167 (2012)
- Alfryyan, N., Alrowaili, Z.A., Alomairy, S., Nabil, I.M., Al-Buriahi, M.S.: Radiation attenuation properties of zinc-borosilicate glasses containing Al₂O₃ and Gd₂O₃. *SILICON* **15**, 8031–8043 (2023)
- Alrowaili, Z.A., Khattari, Z.Y., Alsaif, N.A.M., Shams, M.S., El-Refaei, A.M., Elsad, R.A., Al-Buriahi, M.S., Rammah, Y.S.: Synthesis, physical properties, neutron, and gamma-ray shielding competence of borate-based glasses reinforced with erbium (III) oxide: a closer-look on the impact of Eu₂O₃. *J. Mater. Sci. Mater. Electron.* **34**, 221–231 (2023)
- Alsaif, N.A.M., Ahmed, M.M., Al-Ghamdi, H., El-Hamalawy, A.A., Adawy, W.M., Rammah, Y.S., Ahmad, S.K.: Fabrication, physical and machine learning density prediction techniques of newly B₂O₃–ZnO–BaO–PbO glasses. *Opt. Mater.* **142**, 113994–114002 (2023c)
- Alsaif, N.A.M., Ahmmad, S.K., Khattari, Z.Y., Abdelghany, A.M., El-Refaei, A.M., Rammah, Y.S., Shams, M.S., Elsad, R.A.: Synthesis, structure, radiation attenuation efficacy as well as prediction of density using artificial intelligence techniques of lead borate lithium zinc strontium glasses. *Opt. Mater.* **137**, 113599–113606 (2023a)
- Alsaif, N.A.M., Elsad, R.A., Sadeq, M.S., Rammah, Y.S., Ahmed, E.M., El-Hamalawy, A.A., Shams, M.S.: Antimony (III) oxide-reinforced lithium-calcium borate glasses: preparation and characterization of physical, optical, and γ -ray shielding behavior through experimental and theoretical methods. *J. Electron. Mater.* **51**, 5869–5879 (2022)
- Alsaif, N.A.M., Khattari, Z.Y., Shams, M.S., Rammah, Y.S., El-Refaei, A.M., Elsad, R.A.: Elastic-mechanical, dielectric properties, and γ -radiation safety competence of calcium boro-zinc glass systems reinforced with Nb⁵⁺ ions: experimental and theoretical studies. *J. Mater. Sci. Mater. Electron.* **34**, 402–411 (2023b)
- Arya, S.K., Singh, K.: Structural and optical properties of 30Li₂O–55B₂O₃–5ZnO–xTiO₂–(10–x)V₂O₅, (0 \leq x \leq 10) glasses. *J. Non-Cryst. Solids* **414**, 51–58 (2015)
- Bashter, I.: Calculation of radiation attenuation coefficients for shielding concretes. *Ann. Nucl. Energy* **24**, 1389–1401 (1997)
- Brown, F.B., et al.: MCNP version 5. *Trans. Am. Nucl. Soc.* **87**(273), 02–3935 (2002)
- Davis, E.A., Mott, N.: Conduction in non-crystalline systems V. Conductivity, optical absorption and photoconductivity in amorphous semiconductors. *Philos. Mag.* **22**(179), 0903–0922 (1970)
- Ekinci, N., Mahmoud, K., Aygün, B., Hessien, M., Rammah, Y.: Impacts of the colemanite on the enhancement of the radiation shielding capacity of polypropylene. *J. Mater. Sci. Mater. Electron.* **33**, 20046–20055 (2022)
- Hassaan, M.Y., Osman, H.M., Hassan, H.H., Helal, M.A., El-Dee, A.S.: Enhancing the electrical conduction in sodium borosilicate titanate glass doped with Nd or Gd ions to increase its optical absorption for smart windows applications. *Optik – Int. J. Light Electron Opt.* **185**, 477–485 (2019)
- Hassib, M.D., Kaky, K.M., Kumar, A., Şakar, E., Sayyed, M.I., Baki, S.O., Mahdi, M.A.: Boro-silicate glasses co-doped Er⁺³/Yb⁺³ for optical amplifier and gamma radiation shielding applications. *Phys. B Condens. Matter* **567**, 37–44 (2019)

- Ibrahim, A.K., Bondouk, I., Allam, E.A., Nabil, I.M., Al-Abyad, M., Saudi, H., El-TaHER, A., Mahmoud, M.E., Amar, A.: A binary composite material of nano polyaniline intercalated with nano-Fe₂O₃ for enhancing gamma-radiation-shielding properties: experimental and simulation study. *Progress Nucl. Energy* **169**, 105067–105077 (2024)
- Kaky, K.M., Lakshminarayana, G., Baki, S.O., Halimah, M.K., Mahdi, M.A.: Structural, thermal and optical studies of bismuth doped multicomponent tellurite glass. *Solid State Phenom.* **268**, 165–171 (2017)
- Kaky, K.M., Sayyed, M.I.: Selected germanate glass systems with robust physical features for radiation protection material use. *Radiat. Phys. Chem.* **215**, 111321–111329 (2024)
- Kaky, K.M., Sayyed, M.I., Mhareb, M.H.A., Abbas, H.H., Baki, S.O.: Physical, structural, mechanical, and various radiation shielding properties of TeO₂-GeO₂-ZnO-Al₂O₃-Li₂O-M (M= WO₃, MoO₃, PbO, and CuO) glasses. *Opt. Mater.* **145**, 114370–114377 (2023)
- Kaky, K.M., Şakar, E., Akbaba, U., Emre Kasapoğlu, A., Sayyed, M.I., Gür, E., Baki, S.O., Mahdi, M.A.: X-ray photoelectron spectroscopy (XPS) and gamma-ray shielding investigation of boro-silicate glasses contained alkali/alkaline modifier. *Res. Phys.* **14**, 102438–102445 (2019)
- Kawa M. Kaky, M.I. Sayyed, Abbas Khammas, Ashok Kumar, Erdem Şakar, Alyaa H. Abdalsalam, Betül Çeviz Şakar, Bünyamin Alim, M.H.A. Mhareb, Theoretical and experimental validation gamma shielding properties of B₂O₃-ZnO-MgO-Bi₂O₃ glass system. *Materials Chemistry and Physics* **242**, 122504–122510 (2020)
- Khattari, Z.Y., Alsaif, N.A.M., Rammah, Y.S., Abou Hussein, E.M., Shams, M.S., Elsad, R.A.: Fabrication, physical, mechanical, and radiation protection properties of bismo-borate glasses containing La³⁺+ Eu³⁺ as additive ions. *Radiat. Phys. Chem.* **201**, 110454–110462 (2022a)
- Khattari, Z.Y., Alsaif, N.A.M., Rammah, Y.S., Shams, M.S., Elsad, R.A.: Physical, elastic-mechanical and radiation shielding properties of antimony borate–lithium in the form B2O3-CaO-Li2O-Sb2O3: experimental, theoretical and simulation approaches. *Appl. Phys. A* **128**(9), 796–806 (2022b)
- Khattari, Z.Y., Zakaly, H.M.H., Alrowaily, A.W., Ene, A., Shams, M.S., Issa, S.A.M., Elsad, R.A., Rammah, Y.S.: A comprehensive study on optical, physical, mechanical and radiation shielding properties of calcium bismuth borophosphate glass–ceramics with distinct V₂O₅ contents. *Opt. Quant. Electron.* **56**(10), 1–23 (2024)
- Lakshminarayana, G., Kaky, K.M., Jedryka, J., El-Naggar, A.M., Albassam, A.A., Myronchuk, G., Mahdi, M.A.: Laser induced elastooptics in novel Bi₂O₃, and Pr₂O₃ doped tellurite rich glasses. *Mater. Lett.* **183**, 322–324 (2016)
- Lakshminarayana, G., Sayyed, M.I., Baki, S.O., Lira, A., Dong, M.G., Kaky, K.M., Kityk, I.V., Mahdi, M.A.: Optical absorption and gamma-radiation-shielding parameter studies of Tm³⁺-doped multicomponent borosilicate glasses. *Appl. Physics A* **124**, 1–16 (2018)
- M.C. Team.: MCNP—a general Monte Carlo N-Particle transport code (X-5 Monte Carlo Team, version 5). Vol. I: overview and theory. Los Alamos National Laboratory, Los Alamos, NM, LA-UR-03-1987 (2003)
- Mansour, S.F., Wageh, S., Alotaibi, M.F., Abdo, M.A., Sadeq, M.S.: Impact of bismuth oxide on the structure, optical features and ligand field parameters of borosilicate glasses doped with nickel oxide. *Ceram. Int.* **47**, 21443–21449 (2021)
- Mariselvam, K.: Physical, optical and radiation shielding features of Yb³⁺ ions doped H₃BO₃ - Bi₂O₃ - BaCO₃ - CaF₂ - ZnO glasses. *Optik – Int. J. Light Electron Opt.* **230**, 166319–166331 (2021)
- Mariselvam, K., Arun kumar, R.: The emission characteristics of Er³⁺: BBFB glasses for infra-red laser and gamma ray shielding applications. *Optik* **226**, 165910–165926 (2021)
- Mariselvam, K., Liu, J.: Concentration effect of Tm³⁺ ions doped B₂O₃-Li₂CO₃-BaCO₃-CaF₂-ZnO glasses: blue laser and radiation shielding investigations. *Opt. Laser Technol.* **154**, 108262–108274 (2022)
- Marzouk, S.Y., Azooz, M.A., Elsaghier, H.M., Zidan, N.A., Abbas, W.: Structural and optical properties of barium titanium borate glasses doped with ytterbium. *J. Mater. Sci. Mater. Electron.* **33**, 18054–18071 (2022)
- Marzouk, M.A., ElBatal, F.H., ElBatal, H.A.: Effect of TiO₂ on the optical, structural and crystallization behavior of barium borate glasses. *Opt. Mater.* **57**, 14–22 (2016)
- Mhareb, M.H.A., Alqahtani, M., Alajerami, Y.S.M., Alshahri, F., Sayyed, M.I., Mahmoud, K.A., Saleh, N., Alonizan, N., Al-Buriah, M.S., Kaky, K.M.: Ionizing radiation shielding features for titanium borosilicate glass modified with different concentrations of barium oxide. *Mater. Chem. Phys.* **272**, 125047–125055 (2021)
- Misbah, M.H., Shams, M.S., Ahmed, E.M., Elsad, R.A., Abdel-Aziz, A.M., Olarinoy, I.O., Rammah, Y.S.: Preparation, structural, optical characteristics, and photon/neutron attenuation competence of sodium fluoroborate glasses: experimental and simulation investigation. *J. Mater. Sci. Mater. Electron.* **33**, 16334–16347 (2022)
- Mosorov, V., Abdullah, J.: MCNP5 code in radioactive particle tracking. *Appl. Radiat. Isot.* **69**, 1287–1293 (2011)
- Mostafa, A.M.A., Zakaly, H.M.H., Al-Ghamdi, S.A., Issa, S.A.M., Al-Zaibani, M., Ramadan, R.M., El Agammy, E.F.: PbO-Sb₂O₃-B₂O₃-CuO glassy system: evaluation of optical, gamma and neutron shielding properties. *Mater. Chem. Phys.* **258**, 123937–12397 (2021)

- Nabil, I.M., El-Samrah, M.G., Omar, A., Tawfic, A.F., El Sayed, A.F.: Experimental, analytical, and simulation studies of modified concrete mix for radiation shielding in a mixed radiation field. *Sci. Rep.* **13**(1), 17637–17652 (2023)
- Nageswara Raoa, P., Laxmi Kanthb, C., Krishna Raoa, D., Veeraiha, N.: Influence of titanium ions on optical properties of AF–PbO–B₂O₃ glasses. *J. Quant. Spectrosc. Radiat. Transf.* **95**, 373–386 (2005)
- Negm, H.H., Abdo, M.A., Sadeq, M.S.: Impact of Y₂O₃ on structural, mechanical and nonlinear optical properties of CrO₃–Na₂O–B₂O₃ glasses. *Optik-Int. J. Light Electron Opt.* **274**, 170546–170554 (2023)
- Rammah, Y.S., Al-Buriah, M.S., Sriwunkum, C., Shams, M.S., Yousef, E.: Influence of Er³⁺-doped ions on the linear/nonlinear optical characteristics and radiation shielding features of TeO₂–ZnO–Er₂O₃ glasses. *J. Mater. Sci. Mater. Electron.* **31**, 21431–21443 (2020a)
- Rammah, Y.S., Alsaif, N.A.M., Khattari, Z.Y., Shams, M.S., Elsad, R.A., Sadeq, M.S.: Synthesis, physical, FTIR, and optical characteristics of B₂O₃–CaO–ZnO glasses doped with Nb₂O₅ oxide: experimental investigation. *J. Mater. Sci. Mater. Electron.* **33**, 23749–23760 (2022)
- Rammah, Y.S., Mahmoud, K., El-Agawany, F., Tashlykov, O., Yousef, E.: Tm³⁺ ions-doped phosphate glasses: nuclear shielding competence and elastic moduli. *Appl. Phys. A* **126**, 1–11 (2020b)
- Sadeq, M.S., Ibrahim, A.: The path towards wide-bandgap and UV-transparent lithium phosphate glasses doped with cobalt oxide for optical applications. *J. Non-Cryst. Solids* **569**, 120983–120091 (2021)
- Sakar, E., Özgür, F., Bünyamin, A., Sayyed, M.I., Murat, K.: Phy-X/PSD: Development of a user friendly online software for calculation of parameters relevant to radiation shielding and dosimetry. *Radiat. Phys. Chem.* **166**, 108496–108507 (2020)
- Saleh, A., Elshazly, R., Abd Elghany, H.: The impact of CdO on the radiation shielding properties of zinc-sodium-phosphate glass containing barium. *Arab. J. Nucl. Sci. Appl.* **55**, 116–126 (2022)
- Salem, M.M., Kenawy, E., Zakaly, H.M.H., Ene, A., Azaam, M.M., Edries, T.B., Zhou, D., Hussein, M.M., Abd El-Hameed, A.S., Nabil, I.M., Darwish, M.A.: Electrospun PVDF/Barium hexaferrite fiber composites for enhanced electromagnetic shielding in the X-band range. *Res. Phys.* **53**, 106975–106988 (2023)
- Sayyed, M.I., Elmosalami, T.A., Abdo, M.A., Sadeq, M.S.: Optical and radiation shielding features of NiO–CdO–BaO borosilicate glasses. *Phys. Scr.* **97**, 085802–085815 (2022)
- Sayyed, M.I., Kaky, K.M., Gaikwad, D.K., Agar, O., Gawai, U.P., Baki, S.O.: Physical, structural, optical and gamma radiation shielding properties of borate glasses containing heavy metals (Bi₂O₃/MoO₃). *J. Non-Crystall. Solids* **507**, 30–37 (2019)
- Shahboub, A., Saleh, A., Hassan, A., Damrawi, G.E.: EPR studies and radiation shielding properties of silver aluminum phosphate glasses. *Appl. Phys. A* **129**, 410–421 (2023)
- Tauc, J.: Optical properties of amorphous semiconductors. In: *Amorphous and Liquid Semiconductors*, pp. 159–220. Springer, Boston (1974)
- Zahran, H.Y., Mohammed, M.I., Yousef, E.S., Alqahtani, M.S., Reben, M., Algarni, H., Umar, A., Albargi, H.B., Yahia, I.S., Abdel-wahab, M.S., Ibrahim, M.A.: Radiation attenuation properties of the quaternary semiconducting compounds Cu₂CoGe[S, Se, Te]₄. *Res. Phys.* **37**, 105488–105488 (2022)
- Zakaly, H.M.H., Ene, A., Olarinoye, I.O., Marzouk, S.Y., Abdel-Hafez, S.H., Shams, M.S., Rammah, Y.S.: Investigation of Er³⁺ ions reinforced zinc-phosphate glasses for ionizing radiation shielding applications. *Materials* **14**, 6769–6781 (2021)
- Zakaly, H.M.H., Nabil, I.M., Issa, S.A.M., Almousa, N., Khattari, Z.Y., Rammah, Y.S.: Probing the elasticity and radiation protection potential of neodymium(III) doped zinc and niobium tellurite glasses: an integrated simulated and applied physics perspective. *Mater. Today Commun.* **37**, 107113–107125 (2023)
- Zhou, W., Cui, T., Zhang, Z., Yang, Y., Yi, H., Hou, D.: Measurement of wide energy range neutrons with a CLYC (Ce) scintillator. *J. Instrum.* **18**, P02014–P02035 (2014)

Publisher's Note Springer Nature remains neutral with regard to jurisdictional claims in published maps and institutional affiliations.

Springer Nature or its licensor (e.g. a society or other partner) holds exclusive rights to this article under a publishing agreement with the author(s) or other rightsholder(s); author self-archiving of the accepted manuscript version of this article is solely governed by the terms of such publishing agreement and applicable law.

Authors and Affiliations

Norah A. M. Alsaif¹ · Nada Alfryyan¹ · Hanan Al-Ghamdi¹ · Adel M. El-Refaey² · R. A. Elsad³ · M. S. Shams^{2,4} · Y. S. Rammah⁵ · M. S. Sadeq^{6,7} · Shaaban M. Shaaban⁸ · Islam M. Nabil⁹

✉ Y. S. Rammah
dr_yasser1974@yahoo.com

Norah A. M. Alsaif
noaalsaif@pnu.edu.sa

Nada Alfryyan
naalfryyan@pnu.edu.sa

Hanan Al-Ghamdi
hmalghmdi@pnu.edu.sa

Adel M. El-Refaey
adel_elrefaey@aast.edu

R. A. Elsad
ragab.elsad@gmail.com

M. S. Shams
mshans_2008@yahoo.com

M. S. Sadeq
msadeq@yahoo.com

Shaaban M. Shaaban
shabaan27@gmail.com

Islam M. Nabil
im2029@fayoum.edu.eg

¹ Physics Department, College of Science, Princess Nourah Bint Abdulrahman University, P.O. Box 84428, 11671 Riyadh, Saudi Arabia

² Department of Basic and Applied Science, College of Engineering and Technology, Arab Academy of Science, Technology and Maritime Transport, Smart Village, Giza, Egypt

³ Basic Engineering Science Department, Faculty of Engineering, Menoufia University, Shebin El-Koom 32511, Egypt

⁴ Physics and Mathematical Engineering Department, Faculty of Electronic Engineering, Menoufia University, Menouf 32952, Egypt

⁵ Department of Physics, Faculty of Science, Menoufia University, Shebin El-Koom 32511, Egypt

⁶ Department of Basic Science, Faculty of Engineering, Sinai University–Kantara Branch, Ismailia 41636, Egypt

⁷ MEU Research Unit, Middle East University, Amman, Jordan

⁸ Department of Electrical Engineering, College of Engineering, Northern Border University, 1321 Arar, Saudi Arabia

⁹ Physics Department, Faculty of Science, Fayoum University, Fayoum, Egypt